nature research

https://doi.org/10.1038/s41578-020-00268-7

Supplementary information

Artificial channels for confined mass transport at the sub-nanometre scale

In the format provided by the authors and unedited

Supplementary Information

Artificial channels for confined mass transport at the sub-nanometre scale

Jie Shen[1,2], Gongping Liu[2], Yu Han[1], Wanqin Jin[2]*

[1] *Physical Sciences and Engineering Division, Advanced Membranes and Porous Materials Center, King Abdullah University of Science and Technology (KAUST), Thuwal, Saudi Arabia.*

[2] *State Key Laboratory of Materials-Oriented Chemical Engineering, College of Chemical Engineering, Nanjing Tech University, 30 Puzhu South Road, Nanjing, P. R. China.*
** e-mail: wqjin@njtech.edu.cn*

Supplementary Table

Supplementary Table S1. Membranes or devices with sub-nm scaled channels for various applications.

Applications	Channel type	Materials and platform	Fabrication methods	Channel structure property	Performance	Mass transport mechanism	Challenges	Proximity to commercialization
Water desalination	Nanopores	UiO-66 MOFs membranes[1]	Solvothermal growth	Pore window size: ~6 Å, ordered, semi-rigid	Al^{3+} rejection: 99.3%, water flux: 0.14 L $h^{-1}m^{-2}$ bar^{-1}	Sieving effect	Thick active layer, cracks and defects	Concept
	Nanopores	Single layer porous graphene[2]	CVD growth followed by depositing CNTs networks and oxygen plasma etching	Pore size: ~5−10 Å, unordered, semi-rigid	In FO process: NaCl rejection: 98.1 ± 0.3%, water flux: 20.6 L $h^{-1}m^{-2}$ bar^{-1} In RO process: NaCl rejection: ~86%, water flux: 97.6 L $h^{-1}m^{-2}$ bar^{-1}	Sieving effect + electrical effect (electrostatic interaction)	Scale-up fabrication, mechanical properties	Concept
	1D nanotubes	CNTs membrane[3]	CVD growth	Pore size: < 20 Å, ordered, rigid	$Fe(CN)_6^{3-}$ rejection: ~ 98%, water flux: 5.4×10^{-3} L $h^{-1}m^{-2}$ bar^{-1}	Electrical effect (electrostatic interaction)	Scale-up fabrication	Concept
		CNTs MMMs[4]	Interfacial polymerization blending with CNTs	Pore size: ~ 10 Å, unordered, zwitterion functionalized, rigid	NaCl rejection: 98.6%, water flux: 1.6 L $h^{-1}m^{-2}$ bar^{-1}	Solution-diffusion	Dispersibility, interfacial defects	Near commercialization
	2D nanochannels	GO membranes[5]	Pressure filtration	Interlayer spacing: ~ 10 Å, easy to be functionalized, semi-rigid	$MgCl_2$ rejection: 98.6%, water flux: 51.2 L $h^{-1}m^{-2}$ bar^{-1}	Electrical effect (electrostatic interaction)	Processability, anti-fouling property	Near commercialization
		rGO membranes[6]	Pressure filtration followed by hydroiodic acid reduction	Interlayer spacing: ~ 3.5 Å, unordered, semi-rigid	In FO process, water flux: 12 L $h^{-1}m^{-2}$, reverse flux of NaCl: 0.2 mol $h^{-1}m^{-2}$, 0.5 mol L^{-1} ammonium bicarbonate as draw solution and 0.1 mol L^{-1} NaCl as feed solution	Sieving effect	Processability	Concept
		GO MMMs[7]	Interfacial polymerization blending with GO	Interlayer spacing: ~ 10 Å, semi-rigid	NaCl rejection: 97%, water flux: 2.53 L $h^{-1}m^{-2}$ bar^{-1}	Solution-diffusion	Dispersibility, interfacial defects	Near commercialization
Gas/vapour separation	Nanopores	2D MFI zeolite nanosheet membranes[8]	Nanocrystal seeded growth	Pore size: 5.8 – 6.8 Å, ordered, highly rigid	*P*-xylene/*o*-xylene separation factor: 8,000, p-xylene permeance: 1.9×10^{-7} mol m^{-2} s^{-1} Pa^{-1}	Sieving effect	Processability	Concept

Applications	Channel type	Materials and platform	Fabrication methods	Channel structure property	Performance	Mass transport mechanism	Challenges	Proximity to commercialization
		2D $Zn_2(bim_4)$ MOFs nanosheet membranes[9]	Ball-milling exfoliation followed by pressure filtration	Pore size: ~3 Å, ordered, semi-rigid	H_2/CO_2 selectivity: >160, H_2 permeance: 1,740 GPU at 200 ^oC	Sieving effect	Processability	Concept
		ZIF-8 MOFs membranes[10]	ALD followed by ligand-vapor treatment	Pore size: ~ 4.0−4.2 Å, ordered, semi-rigid	C_3H_6/C_3H_8 selectivity: 72, C_3H_6 permeance: 8.49 × 10^{-8} mol m^{-2} s^{-1} Pa^{-1} at 7 bar, 35 ^oC	Sieving effect	Processability	Concept
		MOF-5 membranes[11]	Secondary growth	Pore size: ~ 7.8 Å, ordered, semi-rigid	CO_2 permeance: 2.55 × 10^{-7} mol m^{-2} s^{-1} Pa^{-1}, CO_2/CH_4 selectivity: 328; CO_2 permeance: 2.06 × 10^{-7} mol m^{-2} s^{-1} Pa^{-1}, CO_2/N_2 selectivity: 410 at 5 bar, 25 ^oC, CO_2 mole fraction in the feed>80%	Chemical effects (CO_2-philic)	Processability, defects	Concept
		Y-*fum*-**fcu**-MOFs MMMs[12]	Blending with polymers	Pore size: ~ 4.7 Å, ordered, rigid	CO_2+H_2S permeability: 1,057.7 barrer, CO_2+H_2S/CH_4 selectivity: 52.8, at 6.9 bar, 35 ^oC; *n*C_4 permeability: 4.2 barrer, *n*C_4/*i*C_4 selectivity: 35 at 1.72 bar, 75 ^oC	Solution-diffusion + Sieving effect	Dispersibility, interfacial defects	Near commercialization
		PIM-TMN-Trip membrane[13]	Solution-casting	Pore size: ~ 5−10 Å, unordered, semi-rigid	H_2 permeability: 36,200 barrer, H_2/N_2 selectivity: 13.3, O_2 permeability: 6,360 barrer, O_2/N_2 selectivity: 2.3, CO_2 permeability:48,800 barrer, CO_2/N_2 selectivity: 17.9 at 1 bar, 25 ^oC	Solution-diffusion	Processability	Near commercialization
		CMS membranes[14]	Pyrolysis of matrimid polyimide	Pore size: <4.5−5 Å, unordered, rigid	H_2 permeability: ~ 250 barrer, H_2/N_2 selectivity: 640, H_2/CH_4 selectivity: 40,350, CO_2 permeability: ~25 barrer, CO_2/CH_4 selectivity: 3,650, N_2 permeability: 0.4 barrer, N_2/CH_4 selectivity: 63, O_2 permeability: 10 barrer, O_2/N_2 selectivity: 21, at 6.9 bar, 35 ^oC	Solution-diffusion (entropic selectivity) + sieving effect	Processability	Near commercialization
		Single layer porous graphene[15]	Low pressure CVD	Pore size: <3−5 Å, unordered, semi-rigid	H_2 permeance: 1.04 × 10^{-6} mol m^{-2} s^{-1} Pa^{-1}, H_2/CH_4 selectivity: 25.1, at 2 bar, 30 ^oC	Sieving effect	Scale-up fabrication, mechanical properties	Concept

Applications	Channel type	Materials and platform	Fabrication methods	Channel structure property	Performance	Mass transport mechanism	Challenges	Proximity to commercialization
	2D nanochannels	GO membranes[16]	Pressure filtration	In-plane pore size: <3 Å, semi-rigid	H_2 permeance: 1.1 × 10^{-8} mol m^{-2} s^{-1} Pa^{-1}, H_2/CO_2 selectivity: 3,400, H_2/N_2 selectivity: 900, at 0.7 bar, 20 °C	Sieving effect + chemical effects (strong CO_2 adsorption)	Processability	Concept
		GO MMMs[17]	Blending with polymers	Interlayer spacing: ~7 Å, semi-rigid	CO_2 permeability: 100 barrer, CO_2/N_2 selectivity: 91, at 3 bar, 25 °C	Solution-diffusion	Dispersibility, interfacial defects	Near commercialization
Pervaporation	Nanopores	NaA Zeolite membranes[18]	Solvothermal growth	Pore size: ~3.8 Å, ordered, highly rigid	Water flux: 11.5 kg m^{-2} h^{-1}, water/ethanol separation factor: >10,000, 90 wt% ethanol/water mixtures at 70 °C	Solution-diffusion + Sieving effect	Defects	Commercialized, REF. [8]
		T_pTG_{Cl} COFs membranes[19]	Pressure filtration	Pore size: ~4.5−10 Å, unordered, rigid	Water flux: 8.53 kg m^{-2} h^{-1}, water/*n*-butanol separation factor: 3,876, 90 wt% *n*-butanol/water mixtures at 80 °C	Solution-diffusion + Sieving effect	Processability	Concept
	2D nanochannels	Diamine-crosslinked GO membranes[20]	Pressure filtration	Interlayer spacing: 9.3 Å semi-rigid	Water flux: 2.3 kg m^{-2} h^{-1}, water/ethanol separation factor: 4,700, 95 wt% ethanol/water mixtures at 80 °C	Solution-diffusion + Sieving effect	Processability, structure stability	Concept
Organic solvent reverse osmosis	Nanopores	CMS membranes[21]	Pyrolysis of poly(vinylidene fluoride)	Pore size: <7 Å, unordered, rigid, withstand pressure over 100 bar	P-xylene/o-xylene selectivity: 25, p-xylene permeance: ~6 × 10^{-9} mol m^{-2} s^{-1} Pa^{-1} at 22 °C, 14 bar	Solution-diffusion + Sieving effect	Processability	Near commercialization
Isotope separation	Nanopores	Graphene layers (1 square inch size)[22]	CVD	"Porous" for protons and deuteron, rigid	H_2/D_2 separation factor: ~8, hydrogen flux: ~2.25 × 10^{-7} mol m^{-2} h^{-1}	Quantum effects	Scale-up fabrication, mechanical properties, defects	Concept
Heterogeneous catalysis	Nanopores	NaA Zeolite membranes[23]	Solvothermal growth	Pore size: ~3.8 Å, ordered, highly rigid	CO_2 hydrogenation for methanol production, H_2O/CO_2 selectivity: ~11,000 at 250°C and 21 bar, CO_2 conversion (57.2% to 54.8%) and methanol yield (39.8% to 38.1%) stable high-purity methanol (~95 wt %) production for more than 100 hours	Chemical effect (charge-dipole interaction)	Processability, operation stability	Near commercialization
Membrane separator for electrochemical	Nanopores	HKUST-1 MOFs-GO membranes[24]	In-situ growth followed by pressure	Pore size: 9 Å, ordered, semi-rigid	Membrane separator for Li-S batteries, low capacity-fading rates of approximately 0.019%	Sieving effect	Processability	Concept

Applications	Channel type	Materials and platform	Fabrication methods	Channel structure property	Performance	Mass transport mechanism	Challenges	Proximity to commercialization
energy storage (EES)			filtration of GO		per cycle over 1,500 cycles			
	Nanopores	AO-PIM-1 membranes[25]	Solution-casting	Pore size: ~7 Å, unordered, semi-rigid	Membrane separator for aqueous organic flow batteries, high cycling stability with electrochemical capacity retentions of 84.5%, over 200 cycles at 80 mA cm^{-2}, high coulombic efficiencies of >99.8% in argon atmosphere	Sieving effect + chemical effect (enhanced hydrophilic)	Degradation and crossover of organic molecules Processability	Concept
Aqueous proton transport	Nanopores	DNA@ZIF-8 MOFs membrane[26]	Solvothermal growth	Pore size: ~4-4.2 Å, ordered, semi-rigid	0.17 S cm^{-1} at 75 °C, under 97% relatively humidity, direct methanol fuel cells with the membrane exhibit the power density of 9.87 mW cm^{-2}	Chemical effects (enhanced hydrophilic)	Processability	Concept
	2D nanochannels	Sulfonate modified GO membranes[27]	Pressure filtration	Interlayer spacing: ~ 10 Å, semi-rigid	0.33 mS cm^{-1} at 80 °C 100% relatively humidity	Chemical effects (strong acidity and hydration capability)	Processability	Concept
Nanofluidic energy harvesting	2D nanochannels	GO membranes with tuned surface charge polarity[28]	Pressure filtration	Interlayer spacing: ~ 10 Å, semi-rigid	Salinity-gradient power conversion system, power density of 0.77 W m^{-2} with an energy conversion efficiency of 36.6% by mixing 0.5 M NaCl and 0.01 M NaCl aqueous solution	Electrical effects (electrostatic interaction)	Processability, low power density	Concept
Sensing devices	Nanopores	*Fum*-**fcu**-MOF films[29]	In-situ growth	Pore size: ~5 Å, ordered, rigid	Selective H_2S detection to concentrations as low as 100 ppb with a detection limit of 5.4 ppb	Chemical effects	Processability	Concept
	2D nanochannels	rGO membranes[30]	Drop casting	Interlayer spacing: ~ 10 Å, , semi-rigid	Humidity, light and heat sensor with fast response showing curvature and electrical resistance changes	Chemical effects (hydrophilic)	Processability	Concept
Electrochemical actuators	2D nanochannels	MoS_2 membranes[31]	Pressure filtration	Interlayer spacing: < 10 Å, rigid	Strain: 0.5%, stress: 11 Mpa, working frequency: 0.125 Hz and potential window: 0.6 V	Electrical effect	Mechanical properties	Concept

Tp: 1,3,5-triformylphloroglucinol and TGCl: triaminoguanidinium chloride.

Supplementary Box

Supplementary Box S1. Transport fundamentals.

In a liquid environment, typically, when the channel size is larger than 100 nm, fluid transport is well-demonstrated by classical convective flow[32] showing that flux is inversely proportional to the fluid viscosity. Hydrodynamic filtration including microfiltration (MF) and ultrafiltration (UF) are the common processes within this channel range, which separate water and solute based on size exclusion using mechanical pressure difference as the driving force. Some UF separation can work within sub-10 nm range[33]. When smaller than 100 nm, the channels sizes are much larger than molecule size but smaller than the gas mean free path. The effusive flow through the channels follows the Knudsen diffusion[34]. Separation is dependent on the probability of a molecule hitting the channel walls, and the flux is inversely proportional to the square root of the molecular mass.

Transport within a sub-nm channel is driven by difference of chemical potential, thereby, controlled by thermodynamic partitioning (sorption coefficients) and kinetic mobility (diffusion coefficients), rather than hydrodynamic sieving. On the basis of the solution-diffusion theory, the gas permeability is defined as the combination of sorption ($\bar{S}_i$) and diffusion ($\bar{D}_i$) coefficients: $P_i = F_i/(\Delta p/l) = \bar{S}_i\bar{D}_i$, where F_i is the flux of gas i, Δp is the difference of transmembrane partial pressure, l is the membrane thickness. The selectivity of permeated gas i to gas j is defined to: $\alpha_{i,j} = (\bar{S}_i/\bar{S}_j) \times (\bar{D}_i/\bar{D}_j)$, where $\bar{S}_i/\bar{S}_j$and $\bar{D}_i/\bar{D}_j$ are the solubility and diffusivity selectivities, respectively.

When the downstream pressure of the membrane is negligible, S_i can be further obtained from this equation: $\bar{S}_i = c_u/p_{ui}$, where c_u is the adsorbed concentration of gas molecule i in the membrane at the upstream side, p_{ui} is the upstream partial pressure. $\bar{S}_i$ and $\bar{S}_j$ are thus experimentally measured as the secant slope of the respective sorption isotherms using dual-mode model[35], and then $\bar{S}_i/\bar{S}_j$ can be calculated. While $\bar{D}_i$ is roughly defined to $f_i\lambda_i^2/6$, where f_i and λ_i are the random walk jumping frequency and the jump length of gas molecule i, respectively. On the basis of transition-state theory, the diffusivity selectivity is obtained by the following relationship (discussed in the earlier reviews[36]):

$$\frac{\bar{D}_i}{\bar{D}_j} = \frac{\lambda_i^2 f_i}{\lambda_j^2 f_j} = \left[\frac{\lambda_i^2}{\lambda_j^2}\right] \underbrace{\exp\left(\frac{\Delta S^*_{D(i,j)}}{R}\right)}_{\text{Entropic contribution (Shape selectivity)}} \underbrace{\exp\left(-\frac{\Delta H^*_{D(i,j)}}{RT}\right)}_{\text{Enthalpic contribution (Size selectivity)}} \quad (1)$$

This equation introduces exponential difference in free energies of activation, which is $\Delta G^*_{D(i,j)}$, equaling to $\Delta H^*_{D(i,j)} - T\Delta S^*_{D(i,j)}$. $\Delta H^*_{D(i,j)}$ and $\Delta S^*_{D(i,j)}$ are the respectively the differences in

diffusion transition-state enthalpy, H^*, and entropy, S^* for component i versus j. This equation points out that for separating similarly sized molecules ($\left[\frac{\lambda_i^2}{\lambda_j^2}\right]$ ~1), the diffusive selectivity can be divided into an enthalpic and an entropic selectivity. It is considered that the enthalpic selectivity (size-based selectivity) is regulated by the difference in guest molecule size. While the loss of vibrational and rotational modes within the sub-nm channels are responsible for the entropic selectivity (shape-based selectivity)[37]. Such theory provides a basic understanding for the gas molecules transport through different materials. In flexible polymers, for instance, the diffusion selectivity is mainly contributed by enthalpy factor due to the distinct activation energies of molecules entering the size-selective transient gaps. However, the segmental motions of polymer chains cause a distribution of free-volume, making the entropic factor to be negligible. While for rigid nanopores, in addition to the enthalpy part, the entropic factor contributes to the diffusion selectivity by hindering the rotational and vibrational motions of the slightly larger molecules. This entropic factor leads to much higher diffusion selectivity of rigid nanopores than flexible polymer.

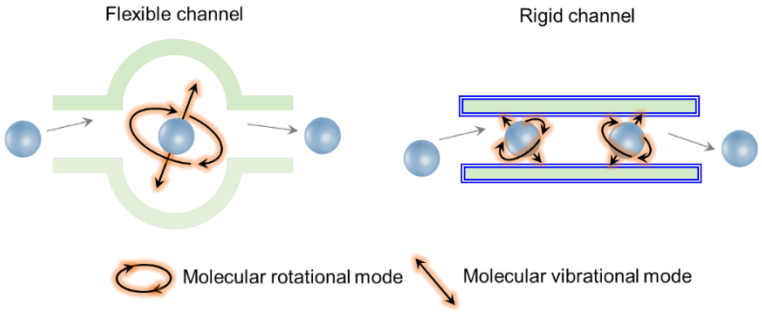

Supplementary Fig. S1. Comparison of molecular transport through flexible and rigid channels.

Water and salt transport in reverse osmosis process also follows solution-diffusion mechanism, with the definition of water flux: $J_w = A(\Delta p - \Delta\pi)$, where J_w is the volumetric water flux, A is the water permeability coefficient, Δp is the applied hydrostatic pressure and $\Delta\pi$ is the osmotic pressure difference across the active layer. The rejection of solute is $R = 1 - (c_p/c_f)$, where c_p and c_f are the solute concentration at permeate side and feed side, respectively. Similar to gas permeation, the solubility and diffusivity jointly determine the water permeability P_w and solute permeability P_s, both of which are independent of layer thickness, reflecting the intrinsic properties of membrane materials. But the diffusion selectivity based on the size difference between water (~3 Å) and monovalent hydrated ions (~6−7 Å) is considered to be the key factor for the overall selectivity[36]. The relationship between A and P_w is depicted as: $A = (P_w V_w)/(\delta RT)$, where V_w is the molar volume of water, δ is the selective layer thickness, R is the gas constant and T is the absolute temperature. Meanwhile, the relationship between solute permeability coefficient B and P_s is: $J_s = (P_s \Delta c_s)/\delta = B\Delta c_s$, where J_s is the solute flux, Δc_s is the solute concentration difference across the selective layer. The performance of selective layer is mainly determined by coefficients A and B [33].

References

1 Liu, X., Demir, N. K., Wu, Z. & Li, K. Highly water-stable zirconium metal–organic framework UiO-66 membranes supported on alumina hollow fibers for desalination. *J. Am. Chem. Soc.* **137**, 6999-7002 (2015).

2 Yang, Y. *et al.* Large-area graphene-nanomesh/carbon-nanotube hybrid membranes for ionic and molecular nanofiltration. *Science* **364**, 1057-1062 (2019).

3 Fornasiero, F. *et al.* Ion exclusion by sub-2-nm carbon nanotube pores. *Proc. Natl. Acad. Sci. U.S.A.* **105**, 17250-17255 (2008).

4 Chan, W.-F. *et al.* Zwitterion functionalized carbon nanotube/polyamide nanocomposite membranes for water desalination. *ACS Nano* **7**, 5308-5319 (2013).

5 Zhang, M. *et al.* Controllable ion transport by surface-charged graphene oxide membrane. *Nat. Commun.* **10**, 1253 (2019).

6 Liu, H., Wang, H. & Zhang, X. Facile fabrication of freestanding ultrathin reduced graphene oxide membranes for water purification. *Adv. Mater.* **27**, 249-254 (2015).

7 Kim, H. J., Lim, M.-Y., Jung, K. H., Kim, D.-G. & Lee, J.-C. High-performance reverse osmosis nanocomposite membranes containing the mixture of carbon nanotubes and graphene oxides. *J. Mater. Chem. A* **3**, 6798-6809 (2015).

8 Jeon, M. Y. *et al.* Ultra-selective high-flux membranes from directly synthesized zeolite nanosheets. *Nature* **543**, 690-694 (2017).

9 Peng, Y. *et al.* Metal-organic framework nanosheets as building blocks for molecular sieving membranes. *Science* **346**, 1356-1359 (2014).

10 Ma, X. *et al.* Zeolitic imidazolate framework membranes made by ligand-induced permselectivation. *Science* **361**, 1008-1011 (2018).

11 Rui, Z., James, J. B., Kasik, A. & Lin, Y. S. Metal-organic framework membrane process for high purity CO2 production. *AIChE J.* **62**, 3836-3841 (2016).

12 Liu, G. *et al.* Mixed matrix formulations with MOF molecular sieving for key energy-intensive separations. *Nat. Mater.* **17**, 283-289 (2018).

13 Rose, I. *et al.* Polymer ultrapermeability from the inefficient packing of 2D chains. *Nat. Mater.* **16**, 932-937 (2017).

14 Zhang, C. & Koros, W. J. Ultraselective carbon molecular sieve membranes with tailored synergistic sorption selective properties. *Adv. Mater.* **29**, 1701631 (2017).

15 Zhao, J. *et al.* Etching gas-sieving nanopores in single-layer graphene with an angstrom precision for high-performance gas mixture separation. *Sci. Adv.* **5**, eaav1851 (2019).

16 Li, H. *et al.* Ultrathin, molecular-sieving graphene oxide membranes for selective hydrogen separation. *Science* **342**, 95-98 (2013).

17 Shen, J. *et al.* Membranes with fast and selective gas-transport channels of laminar graphene oxide for efficient CO_2 capture. *Angew. Chem. Int. Ed.* **54**, 578-582 (2015).

18 Li, J. *et al.* Influences of the zeolite loading and particle size in composite hollow fiber supports on properties of zeolite NaA membranes. *Microporous Mesoporous Mater.* **160**, 10-17 (2012).

19 Yang, H. *et al.* Covalent organic framework membranes through a mixed-dimensional assembly for molecular separations. *Nat. Commun.* **10**, 2101 (2019).

20 Hung, W.-S. *et al.* Cross-linking with diamine monomers to prepare composite graphene oxide-framework membranes with varying d-spacing. *Chem. Mater.* **26**, 2983-2990 (2014).

21 Koh, D.-Y., McCool, B. A., Deckman, H. W. & Lively, R. P. Reverse osmosis molecular differentiation of organic liquids using carbon molecular sieve membranes. *Science* **353**, 804-807 (2016).

22 Lozada-Hidalgo, M. *et al.* Scalable and efficient separation of hydrogen isotopes using graphene-based electrochemical pumping. *Nat. Commun.* **8**, 15215 (2017).

23 Li, H. *et al.* Na^+-gated water-conducting nanochannels for boosting CO_2 conversion to liquid fuels. *Science* **367**, 667-671 (2020).

24 Bai, S., Liu, X., Zhu, K., Wu, S. & Zhou, H. Metal–organic framework-based separator for lithium–sulfur batteries. *Nat. Energy* **1**, 16094 (2016).

25 Tan, R. *et al.* Hydrophilic microporous membranes for selective ion separation and flow-battery energy storage. *Nat. Mater.* **19**, 195-202 (2020).

26 Guo, Y. *et al.* A DNA-threaded ZIF-8 membrane with high proton conductivity and low methanol permeability. *Adv. Mater.* **30**, 1705155 (2018).

27 He, G. *et al.* Bioinspired ultrastrong solid electrolytes with fast proton conduction along 2D channels. *Adv. Mater.* **29**, 1605898 (2017).

28 Ji, J. *et al.* Osmotic power generation with positively and negatively charged 2D nanofluidic membrane pairs. *Adv. Funct. Mater.* **27**, 1603623 (2017).

29 Yassine, O. *et al.* H_2S sensors: fumarate-based fcu-MOF thin film grown on a capacitive interdigitated electrode. *Angew. Chem. Int. Ed.* **55**, 15879-15883 (2016).

30 Cheng, H. *et al.* One single graphene oxide film for responsive actuation. *ACS Nano* **10**, 9529-9535 (2016).

31 Acerce, M., Akdoğan, E. K. & Chhowalla, M. Metallic molybdenum disulfide nanosheet-based electrochemical actuators. *Nature* **549**, 370-373 (2017).

32 Holt, J. K. *et al.* Fast mass transport through sub-2-nanometer carbon nanotubes. *Science* **312**, 1034-1037 (2006).

33 Werber, J. R., Osuji, C. O. & Elimelech, M. Materials for next-generation desalination and water purification membranes. *Nat. Rev. Mater.* **1**, 16018 (2016).

34 Pandey, P. & Chauhan, R. Membranes for gas separation. *Prog. Polym. Sci.* **26**, 853-893 (2001).

35 Vieth, W. R., Howell, J. M. & Hsieh, J. H. Dual sorption theory. *J. Membr. Sci.* **1**, 177-220 (1976).

36 Koros, W. J. & Zhang, C. Materials for next-generation molecularly selective synthetic membranes. *Nat. Mater.* **16**, 289-297 (2017).

37 Jue, M. L., Koh, D.-Y., McCool, B. A. & Lively, R. P. Enabling widespread use of microporous materials for challenging organic solvent separations. *Chem. Mater.* **29**, 9863-9876 (2017).